ADVANCED FUNCTIONAL MATERIALS
www.afm-journal.de

Materials Views
www.MaterialsViews.com

Improved CO_2 Capture from Flue Gas by Basic Sites, Charge Gradients, and Missing Linker Defects on Nickel Face Cubic Centered MOFs

*Elena López-Maya, Carmen Montoro, Valentina Colombo, Elisa Barea, and Jorge A. R. Navarro**

The adsorptive properties of the isoreticular series $[Ni_8(OH)_4(H_2O)_2(BDP\_X)_6]$ (H_2BDP_X = 1,4-bis(pyrazol-4-yl)benzene-4-X with X = H (1), OH (2), NH_2 (3)) can be enhanced by postsynthetic treatment with an excess of KOH in ethanol. In the case of X = H, NH_2, this treatment leads to partial removal of the organic linkers, deprotonation of coordinated water molecules and introduction of extraframework cations, giving rise to materials of $K[Ni_8(OH)_5(EtO)(H_2O)_2(BDP\_X)_{5.5}]$ (1@KOH, 3@KOH) formulation, in which the original framework topology is maintained. By contrast, the same treatment with KOH in the $[Ni_8(OH)_4(H_2O)_2(BDP\_OH)_6]$ (2) system, enclosing the more acidic phenol residues, leads to a new material containing a larger fraction of missing linker defects and extra-framework cations as well as phenolate residues, giving rise to the material $K_3[Ni_8(OH)_3(EtO)(H_2O)_6(BDP\_O)_5]$ (2@KOH), which also conserves the original face cubic centered (fcu) topology. It is noteworthy that the introduction of missing linker defects leads to a higher accessible pore volume with a concomitant increased adsorption capacity. Moreover, the creation of coordinatively unsaturated metal centers, charge gradients, and phenolate nucleophilic sites in 2@KOH gives rise to a boosting of CO_2 capture features with increased adsorption heat and adsorption capacity, as proven by the measurement of pulse gas chromatography and breakthrough curve measurements of simulated flue gas.

1. Introduction

The increasing levels of anthropogenic CO_2 emissions to the atmosphere are believed to be responsible for global warming.[1] Consequently, the development of efficient technologies for CO_2 capture and storage, in a low energy demanding and economic manner, should help to mitigate this problem. Noteworthy, the CO_2 separation process is the most energy demanding step and contributes to ca. of 70% of the cost of the process. This is particularly the case of using aqueous amine solutions for CO_2 capture in which the high heat capacity of these systems leads to a high regeneration energy cost.[2]

Separation technologies based on adsorption by porous materials may help to diminish the cost of the process. In this regard, zeolite based molecular sieves have a major share in gas purification processes, as a consequence of their crystalline nature which gives rise to selective adsorptive properties.[3]

In the last few years, a new class of crystalline nanoporous materials known as metal–organic frameworks (MOFs) have emerged as an alternative to zeolites due to their fascinating performance in molecular adsorption and catalysis.[4–6] Noteworthy, MOFs have particularly arisen as very promising materials for the selective and reversible capture of CO_2.[7,8] In this regard, surface modification of MOFs is a suitable way of enhancing the interaction of CO_2 adsorbate with this material type. In this regard, the literature shows that there are different ways of improving the CO_2 capture by MOFs: i) introduction of coordinatively unsaturated metal sites;[9] ii) incorporation of H-bonding residues[10,11]/charge gradients[12] and iii) functionalization with basic sites.[13–15] An additional way of enhancing the porosity of MOFs is by partial removal of the organic linkers that may open access to previously inaccessible regions as well as the creation of new interaction sites.[16] This is particularly the case of the highly stable face cubic centered (**fcu**) UiO66/UiO67 MOF systems containing $Zr_6O_4(OH)_4$ nodes and linear dicarboxylate linkers in which the treatment with modulating agents leads to porosity improvement as a consequence of the creation of missing linker defects.[17,18]

It should be noted that in addition to the remarkable high adsorptive performance of MOF materials, it is necessary that they meet the requirements for practical applications, namely that they have robust structural frameworks able to resist the highly demanding conditions found in practical applications such as exposure to moisture, acidic or basic environments as well as to high

E. López-Maya, Dr. C. Montoro, Dr. E. Barea, Prof. J. A. R. Navarro
Universidad de Granada
Departamento de Química Inorgánica
18071, Granada, Spain
E-mail: jarn@ugr.es
Dr. V. Colombo
Università di Milano
Dipartimento di Chimica
Via Golgi 19, 20133, Milano, Italy

DOI: 10.1002/adfm.201400795

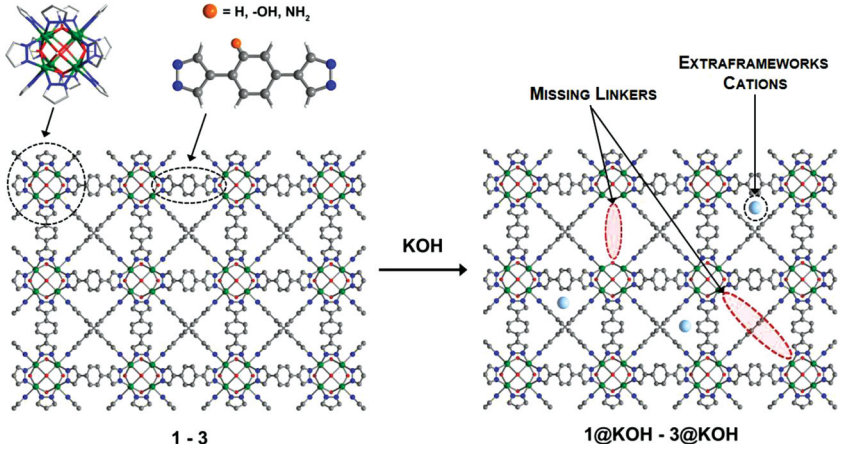

Figure 1. Postsynthetic functionalization of the **fcu** framework $[Ni_8(OH)_4(H_2O)_2(BDP\_X)_6]$ systems (**1**, X = H; **2**, X = OH; **3**, X = NH_2) with KOH to yield the $K[Ni_8(OH)_5(EtO)(H_2O)_2(BDP\_X)_{5.5}]$ (**1@KOH**, **3@KOH**) and $K_3[Ni_8(OH)_3(EtO)(H_2O)_6(BDP\_O)_5]$ (**2@KOH**) systems. Highlighted the local stereochemistry of the octametallic node and the functionalized pyrazolate-based ligand. Green, nickel; red, oxygen; blue, nitrogen; gray, carbon. Hydrogen atoms are omitted for clarity.

temperature and pressure. In this regard, archeotypical MOFs as $[Zn_4O(dbc)_3]$ (MOF-5) or $[Cu_3(btc)_2]$ (HKUST) based on labile coordinative bonds of borderline metal ions with O donor ligands[19] are outperformed by systems of higher stability containing a proper combination of hard metal ions with O-donor ligands[8,20,21] or by those based on robust M–N coordination bonds.[22]

In this context, we have recently shown the formation of an isoreticular series of $[Ni_8(OH)_4(H_2O)_2(L)_6]$ robust MOFs exhibiting the face cubic centered (**fcu**) topology.[23] These systems are based on octanuclear Ni(II) hydroxo clusters of formula $[Ni_8(OH)_4(H_2O)_2]^{12+}$,[24] linked by linear tetradentate bi-pyrazolate or mixed pyrazolate/carboxylate ligands with tunable properties for the capture of harmful volatile organic compounds.

In view of these previous results, we have now explored the CO_2 capture properties of the known $[Ni_8(OH)_4(H_2O)_2(BDP)_6]$ (**1**) (H_2BDP = 1,4-bis(pyrazol-4-yl)benzene) system[23] as well as the novel hydroxo and amino functionalized analogue systems containing the functionalized linkers H_2BDP_OH = 2-hydroxo-1,4-bis(pyrazol-4-yl)benzene (**2**) and $H_2BDP\_NH_2$ = 2-amino-1,4-bis(pyrazol-4-yl)benzene (**3**) (**Figure 1**). Moreover, we have also explored the effect of postsynthetic introduction of missing linkers defects in the MOF framework, charge gradients and basic sites on their CO_2 adsorption properties. These features were generated by postsynthetic treatment of the MOFs with ethanolic solutions of KOH leading to the deprotonation of coordinated water molecules of the $[Ni_8(OH)_4(H_2O)_2]^{12+}$ clusters and/or deprotonation of the hydroxo tags of the BDP_OH linker as well as the generation of missing linkers defects and introduction of extraframework potassium ions without disrupting the original **fcu** topology to yield the systems $K[Ni_8(OH)_5(EtO)(H_2O)_2(BDP\_X)_{5.5}]$ (**1@KOH**, **3@KOH**) and $K_3[Ni_8(OH)_3(EtO)(H_2O)_6(BDP\_O)_5]$ (**2@KOH**) (Figure 1). In the following, the properties and applications for CO_2 capture of the tag functionalized systems (**1–3**) as well as the KOH treated materials (**1@KOH-3@KOH**) will be thoroughly discussed.

2. Results and Discussion

2.1. Synthesis and Characterization

The introduction of the OH and NH_2 tags in the benzene ring of the BDP linkers leads to the reproducible formation of isoreticular **fcu** materials analogous to $[Ni_8(OH)_4(H_2O)_2(BDP)_6]$ (**1**), namely $[Ni_8(OH)_4(H_2O)_2(BDP\_OH)_6]$ (**2**) and $[Ni_8(OH)_4(H_2O)_2(BDP\_NH_2)_6]$ (**3**) as deduced from XRPD patterns (**Figure 2**) and thermogravimetric analyses (see supporting information). The major differences are found in the electronic spectra showing the apparition of a charge transfer band around 425 nm which is particularly evident for the **2** system and should be related to the electron donating nature of the OH and NH_2 groups. On the other hand, the accessibility of guest molecules into the functionalized porous networks was assessed by solid-gas adsorption experiments involving different probe gases, namely, N_2 (77 K) and CO_2 (273 K, 298 K). N_2 adsorption isotherms show that the introduction of the hydroxo and amino tags in the benzene ring in **2** and **3**, respectively, do not hinder the diffusion of this probe molecule. However, the presence of the tags is responsible for a significant diminution of N_2 adsorption capacity of 20 and 33% for **2** and **3**, respectively, as well as a concomitant decrease of the BET surface area (**Figure 3** and **Table 1**) which is consistent with the expected diminution of the pore volume as a consequence of the bulk of the tags.[10] By contrast, the postsynthetic treatment of the **1–3** systems with different excesses of KOH ethanolic solutions is indicative of an increased accessibility to the porous structure as deduced from N_2 adsorption at 77 K (Figure 3 and Figures S9, S11, S13). Noteworthy, this treatment does not disrupt the original **fcu** framework topology as suggested by the maintenance of the XRPD patterns (Figure 2) with only a slight diminution of thermal stability being noticed for **2@KOH** and **3@KOH** materials (Figures S5-S7). The best results are obtained with a large excess of KOH (35 fold) leading to the new materials $K[Ni_8(OH)_5(EtO)(H_2O)_2(BDP\_H)_{5.5}]$ (**1@KOH**), $K_3[Ni_8(OH)_3(EtO)(H_2O)_6(BDP\_O)_5]$ (**2@KOH**) and

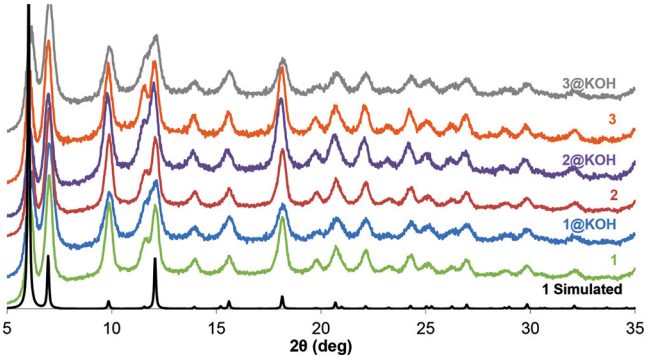

Figure 2. Calculated XRPD pattern for **1** and experimental XRPD patterns for the isoreticular **1**, **2**, **3**, **1@KOH**, **2@KOH** and **3@KOH** materials.

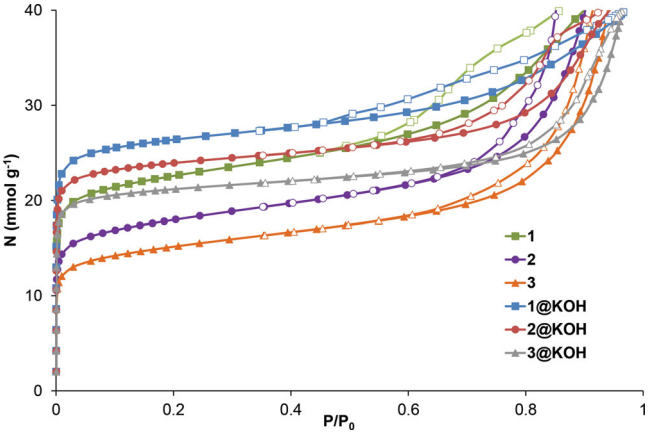

Figure 3. Impact of framework functionalization on N_2 adsorption (77 K) for **1**, **2**, **3**, **1@KOH**, **2@KOH** and **3@KOH**.

$K[Ni_8(OH)_5(EtO)(H_2O)_2(BDP\_NH_2)_{5.5}]$ (**3@KOH**) which introduce potassium extraframework cations and missing linkers defects along with either deprotonated coordinated water molecules (**1@KOH**, **3@KOH**) or deprotonated phenolate residues (**2@KOH**). The introduction of potassium extraframework cations and missing linker defects are consistent with elemental analysis (EA), thermogravimetric (TGA), inductively coupled plasma mass spectrometry (ICP-MS) and transmission electron microscopy (TEM) analyses (see supporting information). In the case of **2@KOH** the electronic spectra shows the apparition of a new broad charge transfer band centered around 800 nm which should be related to a larger electronic delocalization as consequence of the phenol deprotonation. It should also be noted that the missing linker defects do not significantly alter Ni octahedral coordination as can be deduced from the minimal changes in the d-d transitions on passing from **1** to **1@KOH**. This fact should be related to a probable ramdon distribution of linker defects with the pyrazolate coordination positions being replaced by EtOH or water molecules thereby preserving the Ni octahedral environment.

Noteworthy, KOH treated materials exhibit a significant increase in N_2 adsorption capacity and BET surface of 20, 35 and 40% for **1@KOH**, **2@KOH**, **3@KOH**, respectively compared to the pristine **1–3** materials (see Figure 3 and Table 1) which should be related to the higher accessibility of the porous structure as a consequence of the missing linkers defects of small size ligands.[16] It should also be pointed out that the missing pyrazolate ligands will be replaced by coordinated water molecules which after proper activation should lead to the creation of strong binding sites, namely coordinatively unsaturated metal centers.

2.2. CO_2 Capture Properties

2.1.1. Static Adsorption Measurements

Once the systems were characterised we have studied the impact of the introduction of tags as well as missing linker defects, extraframework ions and basic sites on the CO_2 capture properties. In this regard, we have performed static CO_2 adsorption isotherms, pulse gas chromatographic experiments and breakthrough curve measurements employing a simulated flue gas containing 86% of N_2 and 14% of CO_2.

The CO_2 adsorption isotherms reveal that this probe molecule is able to diffuse inside the porous framework of the functionalized systems **1–3** and **1@KOH-3@KOH** (**Figure 4**). The introduction of the polar OH and NH_2 tags has, however, a small impact on the CO_2 adsorption properties with the **1–3** systems behaving similarly which probably should be related to the relative large size of the pore voids. Noteworthy, CO_2 adsorption isotherms for **1@KOH-3@KOH** are indicative of the positive impact of KOH treatment to enhance the CO_2 interaction with the porous framework. This is particularly evident in the isotherms measured at 298 K, which shows an increment of ca. 60% on adsorption capacity on passing from **1** to **1@KOH** and of 100% on passing from **2** and **3** materials to **2@KOH** and **3@KOH** at P = 0.14 bar and 298 K (Figure 3). This improvement can be explained taking into account the following facts: i) the missing linker defects increase the surface area of the materials and concomitantly give rise to coordinatively unsaturated metal centres; ii) the introduction of extraframework cations give rise to charge gradients with the positive impact in the interaction with quadrupolar adsorbates; iii) the creation of phenolate basic sites in **2@KOH** will improve the interaction of CO_2 with the framework surface; iv) in **3@KOH** the presence of H-bonding NH_2 tags will enhance the adsorption of CO_2. As stated in the introduction, all the previous features are of interest in order to apply MOFs materials as adsorbents for removing CO_2 from flue gas.

Table 1. Specific BET Surface Area, Heats of adsorption ΔH_{ads} and Henry constants K_H for CO_2; α CO_2/N_2 partition coefficients calculated from variable-temperature zero-coverage gas chromatography experiments on **1**, **2**, **3**, **1@KOH**, **2@KOH**, **3@KOH**. mmol of CO_2 adsorbed per mmol of MOF from breakthrough experiments of N_2/CO_2 mixtures (0.86:0.14) at 273, 298, and 323 K.

Compound	SA $[m^2g^{-1}]$	$-\Delta H_{ads}$ CO_2 [kJ mol^{-1}]	K_H CO_2 $[cm^3\ m^{-2}]^{a)}$	α	CO_2 273 K	CO_2 298 K	CO_2 323 K
1	1730	23.8	0.03	32	0.51	0.25	0.14
2	1390	23.9	0.07	35	1.00	0.40	0.23
3	1170	27.6	0.14	35	0.86	0.48	0.21
1@KOH	2060	29.4	0.11	55	0.91	0.51	0.27
2@KOH	1830	31.7	0.43	215	2.76	1.16	0.62
3@KOH	1670	31.6	0.17	85	0.80	0.36	0.26

[a)]Calculated values at 298 K.

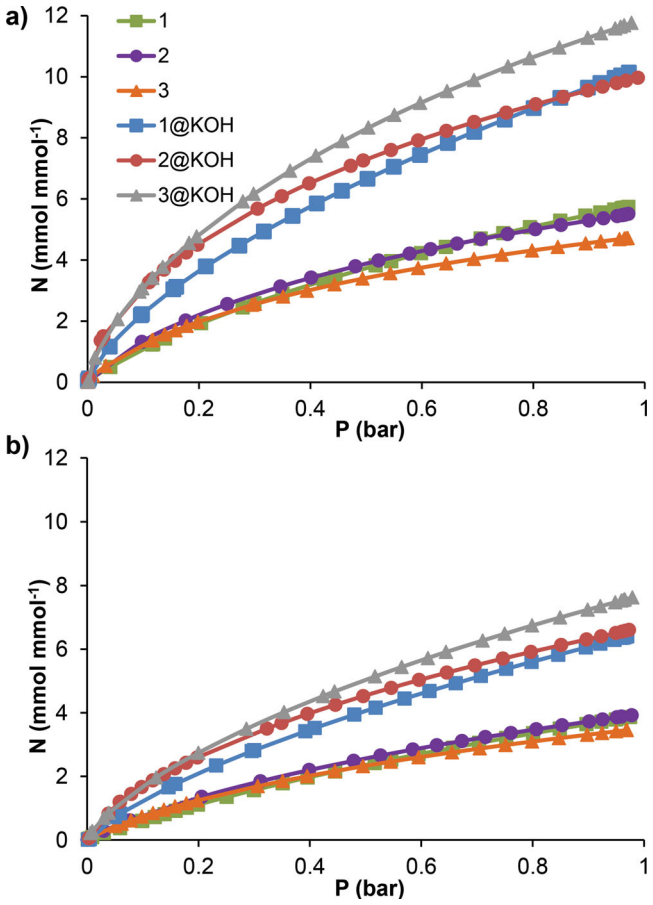

Figure 4. Effect of framework functionalization on CO_2 adsorption at 273 K (a) and 298 K (b). The isotherms are expressed in mmol of adsorbate per formula unit of the materials in order to show the effect of framework functionalization on CO_2 adsorption.

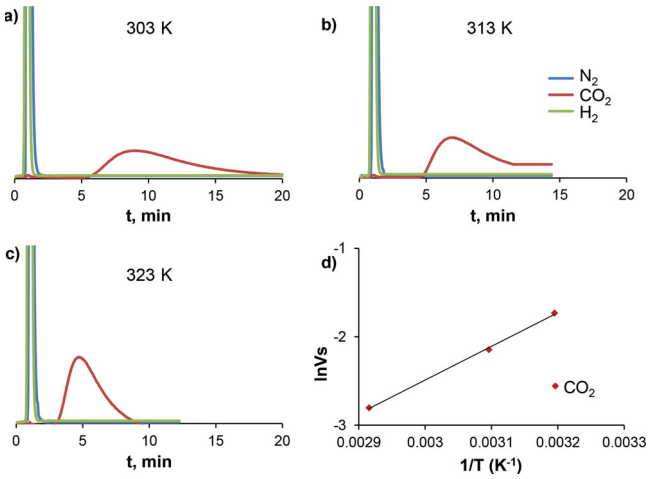

Figure 5. Variable temperature pulse gas chromatograms for equimolecular mixture of H_2, N_2 and CO_2 passed through a chromatographic column packed with **2@KOH**, using a He flow of 30 mL min^{-1} at 303 K (a), 313 K (b) and 323 K (c). Fitting of the variation of the retention volume Vg (in cm^3 g^{-1}) as a function of the adsorption temperature (303–343 K) (d).

2.2.2. Dynamic Adsorption Measurements

In view of the positive effect of the KOH treatment of these materials on CO_2 adsorption, we have studied their gas separation properties by means of pulse gas chromatographic techniques as well as measurement of breakthrough curves.

Variable temperature pulse gas chromatography experiments have been carried out in the 273–353 K temperature range employing the studied MOF materials as adsorption beds of a in house made chromatographic column (see experimental details below) and a pulse of a complex gas mixture (H_2, N_2, CO_2) (**Figure 5**). The results probe the utility of these systems for the capture of CO_2 from flue gas. Indeed, **1**, **2** and **3** materials give rise to significant interaction with carbon dioxide, whereas the interaction with nitrogen and hydrogen molecules is almost negligible. This is manifested by increasing retention times of the essayed gases which follow the trend $H_2 < N_2 << CO_2$ (Figure 5). The differentiated interaction is reflected in high $\alpha_{CO2/N2}$ partition coefficients at room temperature (see Table 1). Noteworthy, the KOH treated materials **1@KOH**, **3@KOH** and particularly **2@KOH** give rise to higher CO_2 adsorption enthalpies as well as much higher $\alpha_{CO2/N2}$ partition coefficients which agree with the positive impact of the presence of coordinatively unsaturated metal centres, charge gradients and basic sites on the interaction with the CO_2 adsorbate (see Table 1).

In order to further highlight the effect of framework functionalization, we have measured breakthrough curves of N_2/CO_2 mixtures with the typical flue gas volumetric composition of 14% in CO_2. The results agree with the strengthening of the interaction of the CO_2 adsorbate upon framework functionalization, which is particularly evident at the typical temperature of flue gas emission (323 K). Indeed, the **1@KOH** and **3@KOH** materials exhibit ca. 2 fold increase in adsorption capacity with regard to the pristine **1** and **3** original materials (Table 1 and **Figure 6**). Noteworthy, **2@KOH** exhibits ca. 5 fold increase in adsorption capacity with regard to the pristine **2** material (Table 1 and Figure 6). The observed performance in adsorption capacity for **2@KOH** materials at the typical temperature of flue gas emission (323 K) is relevant for practical applications in carbon capture technologies and should be related to the synergistic effect of the introduction of missing linkers defects with the concomitant creation of coordinatively unsaturated metal sites, extra-framework cations (charge gradients) and phenolate basic sites. Moreover, the CO_2 capture process by **2@KOH** is highly reproducible over multiple cycles (see Figure 6) and is also low energy demanding, being necessarily heating to 353 K only[9] in order to regenerate the adsorbent. It should be noted, however, that the behavior of the **3@KOH** system in the breakthrough curve tests is below the expected results from the static adsorption measurements which might be attributed to the negative effect of slow diffusion kinetics in the dynamic adsorption process.

3. Conclusions

The incorporation of polar hydroxo and amino tags on the benzene rings of the BDP linkers in the **fcu** framework of **1** is possible giving rise to **2** and **3** isoreticular MOFs. Noteworthy, the postsynthetic treatment of the **1–3** systems with different excesses of KOH ethanolic solutions gives rise to a novel class of materials

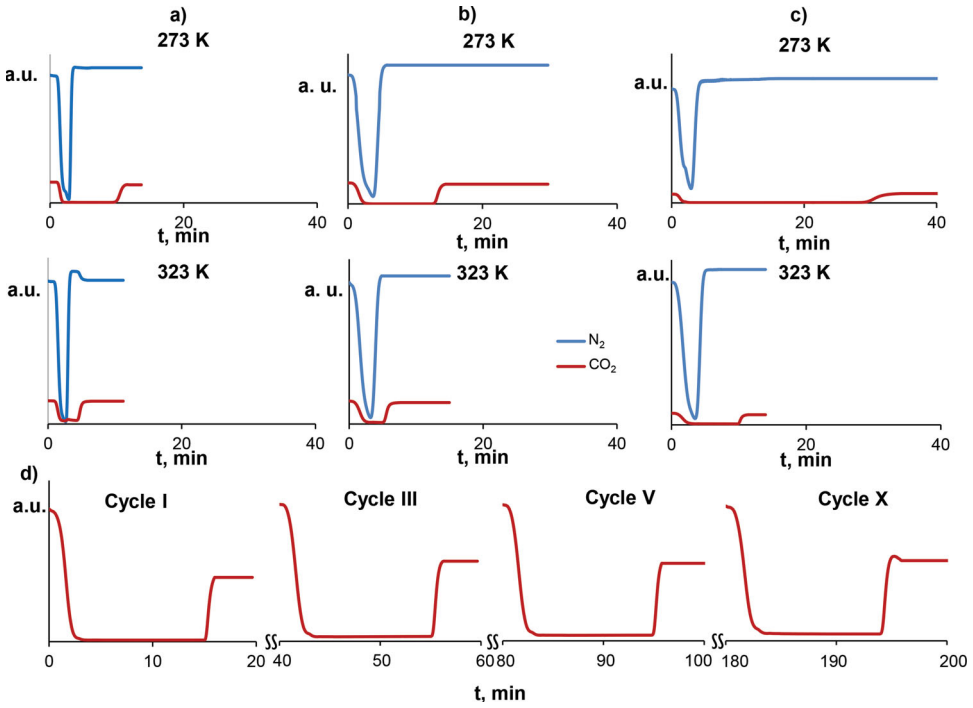

Figure 6. Separation breakthrough experiments of a gas mixture (10 mL min^{-1}) of N_2/CO_2 (86:14 v/v) at 273 K and 323 K, for **1** (a), **2** (b) and **2@KOH** (c) showing the positive effect of introduction of missing linker defects, extraframework cations and basic sites on the CO_2 capture features; (d) successive CO_2 capture breakthrough cycles of **2@KOH** at 298 K with reactivation at 353 K.

1@KOH-3@KOH which maintain the original **fcu** framework topology with an increased accessibility to the porous structure as a consequence of the creation of missing linker defects and the introduction of extraframework cations. These features have a positive impact on the CO_2 capture properties which can be explained taking into account the following facts: i) the missing linker defects increase the surface area of the materials and concomitantly give rise to coordinatively unsaturated metal centers; ii) the introduction of extraframework cations give rise to charge gradients with the positive impact in the interaction with quadrupolar adsorbates; iii) the creation of phenolate basic sites in **2@KOH** improves the interaction of CO_2 with the framework surface; iv) in **3@KOH** the presence of H-bonding NH_2 tags will enhance the adsorption of CO_2. At this point it should be highlighted that the **1@KOH-3@KOH** are unique, as far as we know in the MOFs chemistry, in simultaneously combining at least three of previously mentioned features which synergistically improve the CO_2 capture properties of the adsorbents. Indeed, particularly the **2@KOH** material which combines the i, ii and iii features is able to selectively and reversible capture CO_2 in a low energy demanding process. Future studies will include the effect of cation exchange processes on the gas separation properties of these materials towards acidic gases, as well as the impact of the introduction of missing linkers defects on related isoreticular systems.

4. Experimental Section

4.1. General Methods

All the general reagents and solvents were commercially available and used as received. ^1H NMR were acquired on a 300 MHz Varian Inova Unity Equipment using DMSO as solvent. Thermogravimetric analyses were performed, using a reactive air atmosphere, on a Shimadzu-TGA-50H equipment, at a heating rate of 20 K min^{-1}. XRPD data were obtained on a D2 PHASER Bruker diffractometer using CuKα radiation ($\lambda = 1.5418$ Å) by means of a scan in the 2θ range of 5–35° with 0.05°. The compounds were manually grounded in an agate mortar and then deposited in the hollow of a zero-background silicon sample holder. Adsorption isotherms were measured at 77 K for N_2 and at 273 and 298 K for CO_2, on a Micromeritics Tristar 3000 volumetric instrument. Prior to measurement, powder samples were heated 7 h at 423 K and outgassed to 10^{-1} Pa. K content of the samples was obtained by AA spectroscopic measurements using the Ni content as internal standard. TEM analysis was done using a Philips CM-20 HR electron microscope operating at 200 kV. The TEM samples were prepared by suspending 1 mg of the powder materials in 1 mL of absolute ethanol for 20 minutes to disperse the nanoparticles into the solution and subsequently the materials were hold using a TEM grid (Holey Carbon type) and dipped into the solution for 20 times. Finally they were dried overnight.

4.2. Synthesis

Synthesis of $[Ni_8(OH)_4(H_2O)_2$(1,4-bis(1H-pyrazol-4-yl)benzene$)_6]$ (1), $[Ni_8(OH)_4(H_2O)_2$(2-Hydroxo[1,4-bis(1H-pyrazol-4-yl)benzene$])_6]$ (2) and $[Ni_8(OH)_4(H_2O)_2$(2-Amino[1,4-bis(1H-pyrazol-4-yl)benzene$)_6]$ (3).

Compounds 1–3: These were synthetized according to the published procedure described by us for the preparation of **1**.[12]

Anal. calc. for $Ni_8(OH)_4(H_2O)_2(C_{12}H_8N_4O)_6(H_2O)_{10}$ (**2**): C, 43.16; H, 4.10; N, 17.78; Anal. Found: C, 43.21; H, 4.61; N, 16.92.

Anal. calc. for $Ni_8(OH)_4(H_2O)_2(C_{12}H_9N_5)_6(H_2O)_5$ (**3**): C, 43.39; H, 3.8; N, 21.04; Anal. Found: C, 44.08; H, 4.86; N, 20.88.

Preparation of 1@KOH, 2@KOH, 3@KOH by postsynthetic functionalization with KOH of 1, 2 and 3: First of all, **1**, **2** and **3** materials were thermally activated at 423 K and outgassed to 10^{-1} Pa, in order to obtain the evacuated porous matrix. Afterwards, 0.055 mmol of each material was suspended in 0.35 M KOH absolute ethanol solution

(5.5 mL). The resulting suspensions were stirred overnight under an inert N_2 atmosphere, filtered off and washed copiously with absolute ethanol yielding compounds **1@KOH**, **2@KOH**, **3@KOH**. It should be noted that the variation of the KOH excess do not significantly change the nature of the materials.

Anal. calc. for $K[Ni_8(OH)_3(C_2H_5O)_3(H_2O)_2(C_{12}H_8N_4)_{5.5}](H_2O)_8$ (**1@KOH**): C, 42.80; H, 4.09; N, 15.25; Anal. Found: C, 42.70; H, 4.16; N, 15.71. Calculated residue from TGA for **1@KOH**: $(NiO)_8(K_2O)_{0.5}$: 34.3%; Found: 32.1%. ICP-MS compositions for **1@KOH**: Ni, 404.30 ppm; K, 40.02 ppm.

Anal. calc. for $K_3[Ni_8(OH)_3(C_2H_5O)(H_2O)_6(C_{12}H_7N_4O)_5](H_2O)_5$ (**2@KOH**): C, 37.29; H, 3.28 N, 14.03; Anal. Found: C, 37.57; H, 3.56; N, 14.13. Calculated residue from TGA for **2@KOH**: $(NiO)_8(K_2O)_{1.5}$: 38%; Found: 37.2%. ICP-MS compositions for **2@KOH**: Ni, 260.70 ppm; K, 64.89 ppm.

Anal. calc. for $K[Ni_8(OH)_3(C_2H_5O)_3(H_2O)_2(C_{12}H_9N_5)_{5.5}](H_2O)_6$ (**3@KOH**): C, 41.84; H, 4.07; N, 18.64; Anal. Found: C, 41.62; H, 4.41; N, 19.12. Calculated residue from TGA for **3@KOH**: $(NiO)_8(K_2O)_{0.5}$: 34.4%; Found: 33.8%. ICP-MS compositions for **3@KOH**: Ni, 330.30 ppm; K, 30.30 ppm.

4.3. Dynamic Gas Adsorption Experiments

Variable Temperature Pulse Chromatography: Gas-phase adsorption at zero coverage surface was studied using the pulse chromatographic technique employing a Gas Chromatograph and a glass 15 cm-column (0.4 cm internal diameter) packed with ca. 0.56 g of the studied materials. Prior to measurement, samples were heated overnight at 423 K in a He flow (30 mL min^{-1}). Later on, 1 mL of an equimolecular mixture of H_2, CO_2 and N_2 was injected at 1 bar and the separation performance of the chromatographic column was examined at different temperatures (273 K–303 K) by means of a mass Spectrometer Gas Analysis System (Pfeiffer Vacoon), detecting ion peaks at m/z 44 (CO_2), 28 (N_2), 4 (He) and 2 (H_2). The dead volume of the system was calculated using the retention time of hydrogen as a reference. The zero-coverage adsorption heats (ΔH_{ads}) were derived from the variation of the retention volumes (V_g) as a function of temperature, according to the Clausius-Clapeyron type equation $\Delta H_{ads} = R\Delta(\ln V_g)/\Delta(1/T)$. The direct relation between the retention volume (Vg) and Henry constant (K_H) also permits to calculate the Henry constant values at 298 K (see Table 1). The $\alpha_{CO2/N2}$ partition coefficients have been calculated from the ratio of the Henry constant values for each gas.

Breakthrough Curves: The 15 cm chromatographic columns, prepared as detailed above, were activated under a pure He flow (30 mL min^{-1}) at 423 K for 7 h and then used for evaluating the CO_2/N_2 separation performances of the materials. The desired gas mixture (10 mL min^{-1}) was prepared via mass flow controllers. For instance, CO_2/N_2 (0.14:0.86) mixtures were prepared in order to simulate the emission of flue gas from a power plant employing 1.4 mL min^{-1} of CO_2 and 8.6 mL min^{-1} of N_2 flows, and the breakthrough experiments were carried out, at 273 K, 303 K and 323 K, by step changes from He to CO_2/N_2 flow mixtures. The relative amounts of the gases eluted from the column were monitored on a mass spectrometer gas analysis system (Pfeiffer Vacoon) detecting ion peak at m/z 44 (carbon dioxide), 28 (nitrogen), 4 (helium) and 2 (hydrogen).

Supporting Information

Supporting Information is available from the Wiley Online Library of from the author. It contains XRPD, TGA, IR, TEM images, adsorption isotherms, pulse chromatograms and breakthrough curves.

Acknowledgements

The authors are grateful for the generous support by the Spanish Ministry of Economy (project: CTQ2011–22787 and FPI fellowship to EL) and Junta de Andalucia (P09-FQM-4981).

Received: March 11, 2014
Revised: April 29, 2014
Published online: July 30, 2014

[1] *Special Report on Carbon Dioxide Capture and Storage* (Eds: B. Metz, O. Davidson, H. de Coninck, M. Loos, L. Meyer), Cambridge Univ. Press, Cambridge **2005**.
[2] G. T. Rochelle, *Science* **2009**, *325*, 1652.
[3] *Introduction to Zeolite Science and Practice* (Eds: H. Van Bekkum, E. M. Flanigen, P. A. Jacobs, J. C. Jansen), Elsevier, Amsterdam **2001**.
[4] H. Furukawa, K. E. Cordova, M. O'Keeffe, O. M. Yaghi, *Science* **2013**, *341*, 974.
[5] J.-R. Li, J. Sculley, H.-C. Zhou, *Chem. Rev.* **2012**, *112*, 869.
[6] *Metal-Organic Frameworks: Applications from Catalysis to Gas Storage*, (Ed: D. Farruseng), Wiley-VCH, Weinheim **2011**.
[7] See for example the themed issue on CO_2 separation, capture and reuse in *Chem. Commun.*, available from http://pubs.rsc.org/en/journals/articlecollectionlanding?sercode=cc&themeid=f349f2e2-2e3b-4706-9df7-e77e71bebf90, accessed: July, 2014.
[8] J. Duan, M. Higuchi, S. Horike, M. L. Foo, K. P. Rao, Y. Inubushi, T. Fukushima, S. Kitagawa, *Adv. Funct. Mater.* **2013**, *23*, 3525.
[9] D. Britt, H. Furukawa, B. Wang, T. G. Glover, O. M. Yaghi, *Proc. Natl. Acad. Sci. USA* **2009**, *106*, 20637.
[10] V. Colombo, C. Montoro, A. Maspero, N. Masciocchi, S. Galli, E. Barea, J. A. R. Navarro, *J. Am. Chem. Soc.* **2012**, *134*, 12830.
[11] D.-X. Xue, A. J. Cairns, Y. Belmabkhout, L. Wojtas, Y. Liu, M. H. Alkordi, M. Eddaoudi, *J. Am. Chem. Soc.* **2013**, *135*, 7660.
[12] E. Quartapelle-Procopio, F. Linares, C. Montoro, V. Colombo, A. Maspero, E. Barea, J. A. R. Navarro, *Angew. Chem. Int. Ed.* **2010**, *49*, 7308.
[13] A. Demessence, D. M. D'Alexandro, M. L. Foo, J. R. Long, *J. Am. Chem. Soc.* **2009**, *131*, 8784.
[14] Y. Lin, Q. Yan, C. Kong, L. Chen, *Sci. Report.* **2013**, *3*, 1859.
[15] C. Montoro, E. García, S. Calero, M. Pérez-Fernández, A. L. López, E. Barea, J. A. R. Navarro, *J. Mater. Chem.* **2012**, *22*, 10155.
[16] L. Sarkisov, A. Harrison, *Mol. Simul.* **2011**, *37*, 1248.
[17] H. Wu, Y. S. Chua, V. Krungleviciute, M. Tyagi, P. Chen, T. Yildirim, W. Zhou, *J. Am. Chem. Soc.* **2013**, *135*, 10525.
[18] M. J. Katz, Z. J. Brown, Y. J. Colon, P. W. Siu, K. A. Scheidt, R. Q. Snurr, J. T. Hupp, O. K. Farha, *Chem. Commun.* **2013**, *49*, 9449.
[19] J. A. Greathouse, M. D. Allendorf, *J. Am. Chem. Soc.* **2006**, *128*, 10678.
[20] J. H. Cavka, S. Jakobsen, U. Olsbye, N. Guillou, C. Lamberti, S. Bordiga, K. P. Lillerud, *J. Am. Chem. Soc.* **2008**, *130*, 13850.
[21] F. A. Almeida Paz, J. Klinowski, S. M. F. Vilela, J. P. C. Tomé, J. A. S. Cavaleiro, J. Rocha, *Chem. Soc. Rev.* **2012**, *41*, 1088.
[22] Z. R. Herm, B. M. Wiers, J. A. Mason, J. M. van Baten, M. R. Hudson, P. Zajdel, C. M. Brown, N. Masciocchi, R. Krishna, J. R. Long, *Science* **2013**, *340*, 960.
[23] N. M. Padial, E. Quartapelle Procopio, C. Montoro, E. López, J. E. Oltra, V. Colombo, A. Maspero, N. Masciocchi, S. Galli, I. Senkovska, S. Kaskel, E. Barea, J. A. R. Navarro, *Angew. Chem. Int. Ed.* **2013**, *52*, 8290.
[24] N. Masciocchi, S. Galli, V. Colombo, A. Maspero, G. Palmisano, B. Seyyedi, C. Lamberti, S. Bordiga, *J. Am. Chem. Soc.* **2010**, *132*, 7902.